SOI Suspended membrane waveguide at 3.39 μm for gas sensing application

Muhammad Ali Butt,[*1], Nikolay Lvovich Kazanskiy[1,2]

[1]*Department of Technical Cybernetics, Samara National Research University, 34 Moskovkoye Shosse, Samara 443086, Russia,*
[2]*Institute of RAS-Branch of the FSRC "Crystallography and Photonics" RAS, 151 Molodogvardeiskaya, Samara 443001, Russia.*

Received June 17, 2020; accepted June 25, 2020; published June 30, 2020

Abstract—In this letter, we present a numerical study on designing a silicon-on-insulator (SOI) suspended membrane waveguide (SMW). The waveguide geometry is optimized at 3.39 μm TE-polarized light which is the absorption line of methane gas by utilizing a 3D finite element method (*FEM*). The transmission loss (*TL*) and evanescent field ratio (*EFR*) of the waveguide are calculated for different geometric parameters such as the width of core, height of core and period of the cladding. We found out that *TL* is directly related to *EFR*. Therefore, waveguide geometry can be designed which can offer high *EFR* at the cost of high *TL* or low *EFR* with low *TL*, as desired. Based on the geometric parameters used in this paper, we have obtained a *TL* and *EFR* which lies in the range of 1.54÷3.37dB and 0.26÷0.505, respectively.

In the telecommunication band, the silicon-on-insulator (SOI) platform is generally used for optoelectronic devices [1]. Silicon-based devices are principally appropriate for several applications in the mid-infrared (mid-IR) wavelength range (2 μm - 20 μm), such as on-chip biochemical analysis, in-situ environmental monitoring, and so on. SOI applications are yet inadequate for the buried oxide (BOX) transparent window, which is below 2.6 μm and around 3.4 μm [2]. Several solutions have been proposed for the traditional SOI platform where SiO_2 has been removed [3] or replaced with other materials such as sapphire (Al_2O_3) [4] or silicon nitride (Si_3N_4) [5], respectively. However, typical silicon-on-sapphire (SOS) wafers have more drawbacks, complex fabrication processes, and are more costly than a commercially available SOI wafer. In recent times, suspended membrane waveguide (SMW) with propagation loss as low as 0.8 dB/cm and 3.1 dB/cm have been experimentally demonstrated for λ=3.8 μm and λ=7.67 μm, respectively [6÷7]. SMW, therefore, provides an uncomplicated and efficient approach for mid-IR silicon photonics. This waveguide scheme has numerous advantages including the fabrication on a high-quality SOI wafer using a complementary metal-oxide-semiconductor (CMOS) compatible technology. Due to the micrometre size of mid-IR SMWs, even the standard ultraviolet (UV) photolithography can meet the manufacturing requirements, and accurate size control permits the realization of SMW properties such as dispersion and birefringence. Recently, the mid-IR spectral region has attracted a great deal of interest as it promises the comprehension of several noticeable applications [8÷9] as it possesses absorption peaks of numerous trace gases, such as CH_4, CO, CO_2, NO and NH_3, among others [10]. These gases endure a strong absorbance in the mid-IR region > 2.5μm due to the fundamental rotational and vibrational transitions. In the recent past, several gas sensors have been proposed based on different technologies and platforms, for instance: gas chromatography [11], electrochemical sensors [12], the spectroscopic method [13], among other. Most of these sensor systems are bulky and often pricey. Consequently, they are neither handy nor user-friendly. Under these circumstances, SOI platform based optical waveguides provide an exquisite substitute that entails an evanescent field absorption sensing to detect trace gases. Gas sensors based on evanescent field absorption merely work if the concerned gas has the characteristics absorption line at the operational wavelength. Besides, the gas concentration is directly linked to optical attenuation at a given wavelength [8÷10, 14].

In this letter, we proposed an SOI SMW optimized at 3.39 μm, which is the absorption line of methane (CH_4) gas. Our main aim is to optimize the waveguide geometry that suffers from low transmission loss (*TL*) and offers high evanescent field ratio (*EFR*). SMW design facilitates a large light-matter interaction owing to the extended evanescent field which appears due to the holes in the cladding and lack of the BOX layer. The mode sensitivity of such waveguides is higher than the standard silicon waveguide, which makes them an ideal candidate for mid-IR on-chip spectroscopy. The *TL* is calculated by using the following expression: $TL\ (dB) = 10 \times log\frac{P_{out}}{P_{in}}$, where P_{out} and P_{in} are the output and input power. The

* E-mail: ali_ciit_engineer@yahoo.com

EFR is the proportion of intensity integration of the desired region (upper and lower cladding) and overall intensity integration of the waveguide structure, which is expressed as:

$$EFR = \frac{\iiint_{desired} |E(x,y,z)|^2 dxdydz}{\iiint_{total} |E(x,y,z)|^2 dxdydz}$$

To fabricate these waveguides, a first dry etch step is used to create holes in the silicon layer. The structure is then treated with hydrofluoric (HF) acid, which removes the SiO_2 (BOX) layer through the holes. The silicon waveguide core is then hovering in the air, only supported by a series of silicon strips to the remaining lateral silicon walls. Such silicon strips have an optical purpose besides holding the waveguide core and providing mechanical stability; they act as a subwavelength grating cladding that provides the index contrast necessary for waveguiding [15]. The schematic of SMW is shown in Fig 1. The height and width of the core are denoted as H_{core} and W_{core}, respectively. The width of cladding and height of the BOX layer is labelled as W_{clad} and H_{BOX}, respectively. The cladding period (Λ) is composed of silicon strips (l_{strip}) and holes (l_{hole}) as shown in the inset of Fig.1. The parameters such as H_{BOX}, W_{clad} and number of periods (N) are fixed to shorten the optimization process. In this work, l_{hole} is set to 100 nm, whereas the l_{strip} is varied to obtain variation in Λ. The geometric parameters of the waveguide used in this work are tabulated in Table 1.

Table 1. Geometric parameters of SMW.

W_{core} (nm)	H_{core} (nm)	H_{BOX} (nm)	W_{Clad} (nm)	*Period* (nm)	*a* (nm)	*N*
800 ÷ 1200	400÷600	2000	1400÷1600	300÷600	200	10

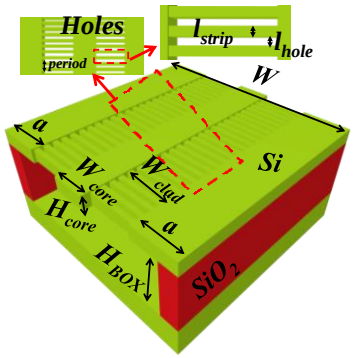

Fig.1. Schematic of an SMW based on SOI platform.

The waveguide model is simulated using COMSOL Multiphysics 5.1 based 3D finite element method (FEM). The electromagnetic (EM) wave frequency domain (*emw*) is chosen as a physics interface. The waveguide model sub-domains are split into triangular mesh elements with a fine mesh grid size of 15 nm for the entire design. The meshing depends on solution accuracy and computational power of the system. This arrangement delivers correct simulation results based on our system processing speed. For wave propagation systems, it is enviable to model a domain with open boundaries of the computational domain as it allows the EM wave to pass through without any reflection. Open geometry is set by assigning scattering boundary conditions (SBC) at the outer edges of the simulation window. At first, the dimensions of the waveguide core are optimized while H_{BOX}, Λ and N are maintained at 2000 nm, 550 nm ($\eta=\frac{l_{hole}}{\Lambda}=0.82$) and 10, respectively. The W_{clad} is in the range of 1000 nm to 1200 nm, which depends on W_{core}. As $W=2a + W_{core} +2W_{clad}$. The *TL* (*dB*) and *EFR* are calculated by varying W_{core} and H_{core}. It is worth noting that loss and *EFR* are directly related to each other. When the dimensions of the waveguide core (W_{core} and H_{core}) increases, it allows the mode to strongly confine in the core. As a result, the losses are reduced up to a certain point and then stabilized as shown in Fig. 2a. However, it reduces the evanescent field power in the cladding, which results in the reduction of *EFR* as shown in Fig.2b. Therefore, there is always a compromise between a strong *EFR* and low *TL*.

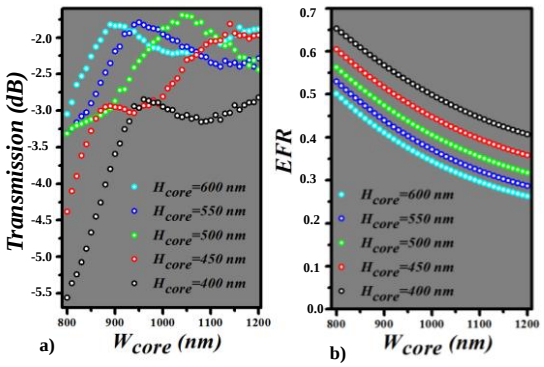

Fig. 2. a) Transmission loss versus waveguide geometry, b) EFR versus waveguide geometry. Λ and H_{BOX} are fixed at 550 nm and 2000 nm.

Afterwards, the effect of cladding Λ on the *TL* and *EFR* is calculated. The parameters such as H_{core} and H_{BOX} are maintained at 600 nm and 2000 nm, respectively. The lowest *TL* and *EFR* of 1.54 dB and 0.35 is obtained at W_{core}=1000 nm and H_{core}= 600 nm. The cladding Λ varies between 300 nm (η=0.67) to 600 nm (η=0.83) and it can be seen that *EFR* is not influenced by the variation in Λ as shown in Fig. 3b. Nevertheless, a higher *EFR* ~ 0.5 can be obtained at W_{core}=800 nm and H_{core}=600 nm for 300 nm <Λ<600 nm at a relatively high *TL*. According to Lambert-Beer law, light propagating through the gas suffers a reduction if it contains the absorption line of that gas. It can be calculated as follows:

$$P = P_o \exp(-\varepsilon\eta CL)$$

where P_o is the incident power which is preset as 20 mW; ε is the gas absorption coefficient which is equal to 8.3

atm^{-1} cm^{-1} for 3.392 μm line of a He–Ne laser [16]; η is the *EFR*; *C* is the concentration of CH_4 gas; *L* is the length of the waveguide which is fixed at 5500 nm and *P* corresponds to the transmission light power after being absorbed by the gas. The transmission power decay versus gas concentration is analyzed by utilizing the waveguide geometric parameters marked in Fig. 3b. The η associated with these parameters is also shown. From Fig.3c, we can observe a decay in the output power with an increasing gas concentration. The decay in power is directly related to η and *L*. The waveguide geometry with H_{core}=600 nm and W_{core}=800 nm provides η=0.505, which provides a decay of 4.12 mW from 100 % of gas concentration present in the surrounding of the waveguide sensor. The efficiency of the gas sensors can be enhanced by utilizing other waveguide structures as a slot waveguide or hybrid plasmonic waveguide [8,14,17,18]. The E_x field distribution of the propagating mode is shown in figure 3d. The W_{core}, H_{core} and Λ are maintained at 1000 nm, 600 nm and 450 nm, respectively. The E-field intensity distribution at the cross-section of the waveguide is shown in Fig. 3e.

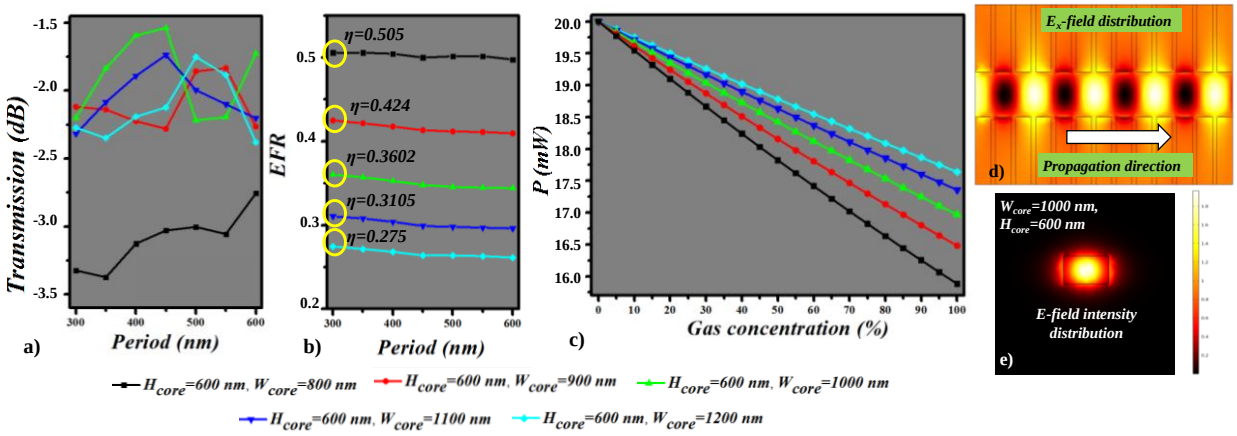

Fig. 3. a) *TL* versus cladding period, b) *EFR* versus cladding period. H_{core} is fixed at 600 nm, c) Output power decay versus gas concentration. The waveguide length (*L*) is fixed to 5500 nm. d) E_x-field distribution in the SMW along the propagation direction, e) E-field intensity distribution at the cross-section of the SMW.

In conclusion, we numerically investigated a suspended membrane waveguide (SMW) based on the silicon-on-insulator platform. The waveguide geometry is optimized at 3.39 μm, which corresponds to the absorption line of methane gas. The dependence of geometric parameters on the transmission loss (*TL*) and evanescent field ratio (*EFR*) is examined for different geometric parameters such as the width of core, height of core and period of the cladding. We found out that *TL* is directly related to *EFR*. Waveguide geometry can be designed, which can provide high *EFR* at the cost of elevated *TL* or low *EFR* with low *TL*, as desired. Based on the geometric parameters used in this paper, we have obtained *TL* and *EFR* which lie in a range of 1.54 dB-3.37 dB and 0.26-0.505, respectively. We believe that our study can provide guidelines for designing low-loss SMWs for mid-infrared applications.

This work was financially supported by the Ministry of Science and Higher Education within the State assignment FSRC «Crystallography and Photonics» RAS (No. 007-GZ/Ch3363/26) for numerical calculations and Russian Science Foundation (No. 20-69-47110) for theoretical results.

References

[1] L. Vivien *et al.*, 16th International conference on transparent optical networks (ICTON), Graz, 2014, pp. 1-4, doi: 10.1109/ICTON.2014.6876536.
[2] Y. Zou, S. Chakravarty, Photonic Research, **6**(4), 254 (2018).
[3] J.S. Penades *et al.*, Opt. Lett. **39**(19), 5661 (2014).
[4] T. Baehr-Jones, A. Spott, R. Ilic, A. Spott, B. Penkov, W. Asher, and M. Hochberg, Opt. Expr. **18**(12),12127 (2010).
[5] J. Mu, R. Soref, L.C. Kimerling, J. Michel, Appl. Phys. Lett. **104**(3), 031115 (2014).
[6] J.S. Penades *et al.*, Optics Lett. **43**(4), 795 (2018).
[7] J.S. Penades *et al.*, Optics Expr. **24**(20), 22908 (2016).
[8] M.A. Butt, S.N. Khonina, N.L. Kazanskiy, Optik **168**, 692 (2018).
[9] S.N. Khonina, N.L. Kazanskiy, M.A. Butt, IEEE Sensors Journal, doi: 10.1109/JSEN.2020.2985840.
[10] M.A. Butt, S.A. Degtyarev, S.N. Khonina, N.L. Kazanskiy, J. Modern Optics **64**(18), 1892 (2017).
[11] S. Zampolli *et al.*, Sensors and Actuators B Chem. **105**(2), 400 (2005).
[12] N. Dossi *et al.*, Lab Chip **12**(1), 153 (2011).
[13] V. Avetisov *et al.*, Sensors, **19**(23), 5313 (2019).
[14] M.A. Butt, S.N. Khonina, N.L. Kazanskiy, Journal of Modern Optics, 65(2), 174-178 (2018).
[15] N.L. Kazanskiy, S.N. Khonina, M.A. Butt, Sensors **20**, 3416 (2020).
[16] H. Tai, H. Tanaka, T. Yoshino, Opt. Lett. **12**, 437 (1987).
[17] M.A. Butt, S.N. Khonina, N.L. Kazanskiy, J. Modern Optics **65**(9), 1135 (2018).
[18] S.A. Degtyarev, M.A. Butt, S.N. Khonina, R.V. Skidanov, International Conference on Computing, Electronic and Electrical Engineering, ICE Cube, Quetta, 2016, pp. 10-13, doi: 10.1109/ICECUBE.2016.7495222.

